

# Deep lithospheric structure across the Central African Shear Zone in Cameroon

J. Plomerová,<sup>1</sup> V. Babuška,<sup>1</sup> C. Dorbath,<sup>2</sup> L. Dorbath<sup>2</sup> and R. J. Lillie<sup>3</sup>

<sup>1</sup>Geophysical Institute, Academy of Sciences of the Czech Republic, Božní II, 141 31 Prague 4, Czech Republic

<sup>2</sup>Institut de Physique du Globe, 5 rue René Descartes, 67084 Strasbourg, France

<sup>3</sup>Department of Geosciences, Oregon State University, Corvallis, Oregon 97331, USA

Accepted 1993 March 16. Received 1992 August 10; in original form 1992 March 6

## SUMMARY

Teleseismic *P*- and *PKP*-arrival times recorded by a network of 40 seismic stations deployed along a 300 km profile across the Adamawa Plateau at the northern end of the Volcanic Line in central Cameroon provide constraints on lithospheric thickness and anisotropy within the subcrustal lithosphere. These data indicate a thinned lithosphere beneath the Central African Shear Zone, where seismologically defined asthenosphere upwells from a depth of about 190 km to about 120 km in a relatively narrow belt. Thus it has only a low-amplitude effect on the observed gravity anomalies; the Bouguer gravity high over the Garoua Rift is consistent with crustal thinning beneath it. An abrupt change of the lithospheric thickness beneath the Northern Boundary Fault correlates with both the topographic relief and a distinct change of the orientation of relatively high- and low-velocity directions, which we infer to be due to anisotropy within the subcrustal lithosphere. This fault may represent an important accretionary suture zone dividing lithospheric blocks that originated in different tectonic settings and acquired different, frozen-in anisotropy.

**Key words:** Cameroon, gravity modelling, lithosphere, *P* residuals.

## 1 INTRODUCTION

This paper describes the deep structure of the lithosphere beneath the Adamawa Plateau, a post-Cretaceous uplifted region on the north-eastern side of the Cameroon Volcanic Line. Although the oldest exposed intrusives show ages of 35–65 Ma, large quantities of basaltic rocks have erupted along the whole length of the volcanic chain in the last 10 Ma; the most recent eruption on Mount Cameroon was in 1982 (Stuart *et al.* 1985). The basement rocks of the Plateau are cut by the West African rift system (Fitton 1983), which can be traced as a series of faults and mylonite zones eastward as the Central African rift system to the western Sudan (Louis 1970). According to De Almeida & Black (1967) the shear zone originated in pre-Cretaceous time, during initial phases of the opening of the South Atlantic, and resulted in a series of subsiding grabens and elongated basins, such as the Djerem-Mbere Basin in the Adamawa region.

By an analysis of teleseismic *P*- and *PKP*-arrival times, the following subjects were addressed: (1) the lithospheric thickness and its changes across the Garoua and Djerem-Mbere rifts (Fig. 1); and (2) differences in

anisotropy within the lithosphere on both sides of the Northern Boundary Fault (NBF).

## 2 DATA AND METHODS

Teleseismic *P*- and *PKP*-arrival times, recorded by 40 vertical short-period stations deployed over a five-month period (Dorbath *et al.* 1986), provide the basis for this study of the deep lithospheric structure in central Cameroon. The region extends from the Garoua Rift in the north through the Adamawa Plateau to Djerem-Mbere in the south (Fig. 1). The relative arrival times recorded during the experiment, from November 1983 to March 1984, were measured by waveform matching across the network, with errors smaller than 0.05 s, and then were converted into absolute traveltimes using the arrival time at the station with the clearest onset of an event. Dorbath *et al.* (1986) analysed these data by the traditional 3-D inversion technique (Aki, Christofferson & Husebye 1977) and plotted variations of the residuals along a N–S profile for different epicentral regions.

In this paper, a different tomographic method (e.g. Babuška, Plomerová & Šilený 1984, 1987a; Babuška,

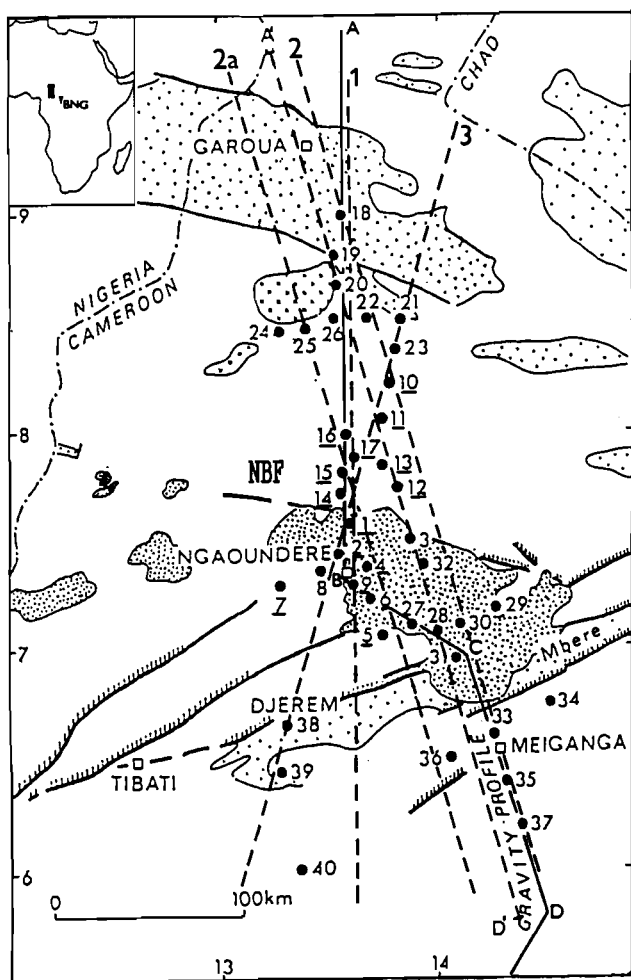


**Figure 1.** Map of the main geological features and the location of seismic stations 1–40. Cambrian and Precambrian basement crystalline rocks (granitoids, migmatites, gneisses and mylonites) are white, volcanites (basalts, andesites, trachytes, phonolites) are densely stippled, Cretaceous sediments (sandstones, conglomerates, marls) are schematically shown by less dense stippling. The Northern Boundary Fault (NBF) is also shown. Fifteen stations used as reference stations in computing relative residuals are underlined. The full line (A–B–C–D) and five dashed lines (1, 2, 2a, 3, A'–D') mark cross-sections through the gravity and lithospheric models (Figs 3–5); locations of the Bangui Observatory (BNG) outside the Adamawa region and the area enlarged in this figure are depicted in the upper left.

Plomerová & Pajdušák 1988) is applied to the same data set, supplemented by the arrival times recorded at a nearby seismological observatory at Bangui (station codes BNG and B CAO). Unlike the traditional 3-D inversions, which use an *a priori* block partition of regions and assume only isotropic wave propagation (Babuška *et al.* 1990), the method used in this paper maps the high- and low-velocity regions without the *a priori* defined block boundaries and shows the *P*-wave anisotropy in the uppermost mantle. The tomographic method applied here estimates the depth of seismologically defined lithosphere–asthenosphere transition and maps the orientations of high-velocity directions within it from two components of the relative residuals, that are computed at each station (*i*): (1) a directionally independent average, a so-called representative average,  $\bar{R}_i$ ; and (2) azimuth-

incidence-angle dependent terms  $\bar{R}_{i,k}$ , where index *k* stands for the *k*th source region. The 131 earthquakes from which the *P* waves were recorded were divided into 38 source regions, each of which is a segment with a size of 10° in epicentral distance and 20° in azimuth from the centre of the network at 7.5°N, 13.9°E. The representative average residuals  $\bar{R}_i = 1/N \sum R_{i,k}$  are computed from steeply incident waves, which arrive from all azimuth intervals (*k*). Values  $R_{i,k} = 1/N_k \sum R_{i,j}$  are average residuals from events in individual source regions (*k* denotes a source region with *N<sub>k</sub>* events, labelled *j*). The method exploits lateral variations of  $\bar{R}_i$  to estimate lateral variations of the lithospheric thickness. The directional terms  $\bar{R}_{i,k}$ , computed as differences between the relative residuals  $R_{i,k}$  and the directional average  $\bar{R}_i$  for the station (Babuška *et al.* 1988) are plotted on a stereographic projection for each station. This procedure emphasizes spatial variations of the relative (normalized) residuals and maps regions with similar orientations of relatively high and low velocities in the lithosphere.

A refraction study in the same area provides information on the crustal structure (Stuart *et al.* 1985). The main result is the large difference of the depth of the Moho (M) discontinuity between the northern part of the region, where the crustal thicknesses do not exceed 23 km, and the southern part, i.e. the Adamawa Plateau, where the crust is about 33 km thick. The data do not constrain, however, the details of how the change in crustal thickness occurs. Therefore, two models of the relief of the M discontinuity were used to calculate the crustal corrections that are introduced to minimize crustal effects beneath stations. In Model A the change is smooth and takes place between stations 14 and 5 (see Fig. 1); in model B the change is abrupt and coincides with the northern edge of the Plateau, between stations 14 and 1.

Computation of the relative residuals, often described as a normalization of the residuals, needs a reference level. Several systems of reference stations have been tested. The mean absolute residual calculated for each event over 15 stations (see Fig. 1, underlined stations) was chosen as the most stable (see also Dorbath *et al.* 1986) and least affected by a directional dependence (see Section 5). We used only those events for which the reference base was formed by at least 10 of the 15 reference stations. Details of the *P*-residual method are discussed, for example, in Babuška *et al.* (1984, 1987a, 1988).

High-quality measurements of correlated PKP arrivals over the array allowed us to modify the method that was, originally, developed for *P* arrivals; we can thereby obtain an independent estimate of the lithosphere–asthenosphere relief from subvertical arrivals. The azimuth–epicentral-distance distribution of 59 PKP sources is less homogeneous than that for *P* waves, but this is not critical owing to the very steep incidence of PKP. The PKP sources were grouped into segments that concentrate around azimuths of 45° and 135°.

Stuart *et al.* (1985) compiled Bouguer gravity anomalies along a profile more than 500 km long and trending N–S in its northern half and NNW–SSE in its southernmost part (see Fig. 1). Following Talwani, Worzel & Landisman (1959), and assuming two-dimensionality, we calculated theoretical gravity anomalies for structures with boundaries

separating media of different densities, i.e. sediments, crust, lower lithosphere and asthenosphere. These zones are shown with density contrasts relative to normal crustal materials. The input data for the initial model are the sediment thicknesses and the M-discontinuity relief (Stuart *et al.* 1985), which include a step of 10 km along the profile (see Figs 5 and 9). The starting model is enlarged here in comparison with traditional crustal gravity modelling by incorporating the relief of the lithosphere–asthenosphere transition derived from *P*-wave delay times (see Section 3).

### 3 MODEL OF LITHOSPHERE THICKNESS

Fairhead & Reeves (1977) presented a tentative lithospheric thickness map of the African continent based on the interpretation of teleseismic delay times and regional Bouguer gravity anomalies. As in previous surface-wave studies (Knopoff & Schlue 1972; Long *et al.* 1972; Dorbath & Montagner 1983), *P* residuals indicated that the African lithosphere–asthenosphere transition varies considerably in depth. As most seismological stations are close to seismically active zones, the large-scale map of lithospheric thickness also was derived (Fairhead & Reeves, 1977) from residuals predicted from the theory of isostasy, according to which the variations in thicknesses of a low-density and a presumed low *P*-velocity compensating body should be reflected in the teleseismic delay-time data. Undulations of

the lithosphere–asthenosphere transition seem to be more pronounced in the south-eastern part of Africa, whereas the lithosphere in the central and north-western parts is estimated as being thicker, on average, and flatter at its base (Fairhead & Reeves, 1977).

Lithospheric thicknesses presented here are limited to a much smaller region, approximately  $200 \times 400$  km, situated north-westward of Bangui (BNG) seismological observatory (see Fig. 1), which we use as a reference station for computing lithospheric thickness. Fig. 2 shows the distribution of the directionally independent averages ( $\bar{R}_i$ ) computed for *P* and *PKP* waves (Table 1). The distribution is fairly consistent for both types of waves: the three northernmost stations of the array and all the stations south of the Northern Boundary Fault (NBF) have negative representative average residuals, whereas the stations north of the fault in the central part of the array have slightly positive residuals. The residuals range from  $-0.6$  s to  $+0.3$  s. This difference of almost 1 s exceeds by an order of magnitude the common mean errors of the residuals (Table 1) within the array.

Because we work with the relative residuals corrected for crustal effects, the effects of lateral variations in velocity in deep mantle paths and focal regions are minimized by the normalization (e.g. Babuška *et al.* 1984), and sources of residual variations are thought to originate in the upper mantle. This is supported by the practically identical patterns of  $\bar{R}_i$  over the array for both *P* and *PKP* waves,

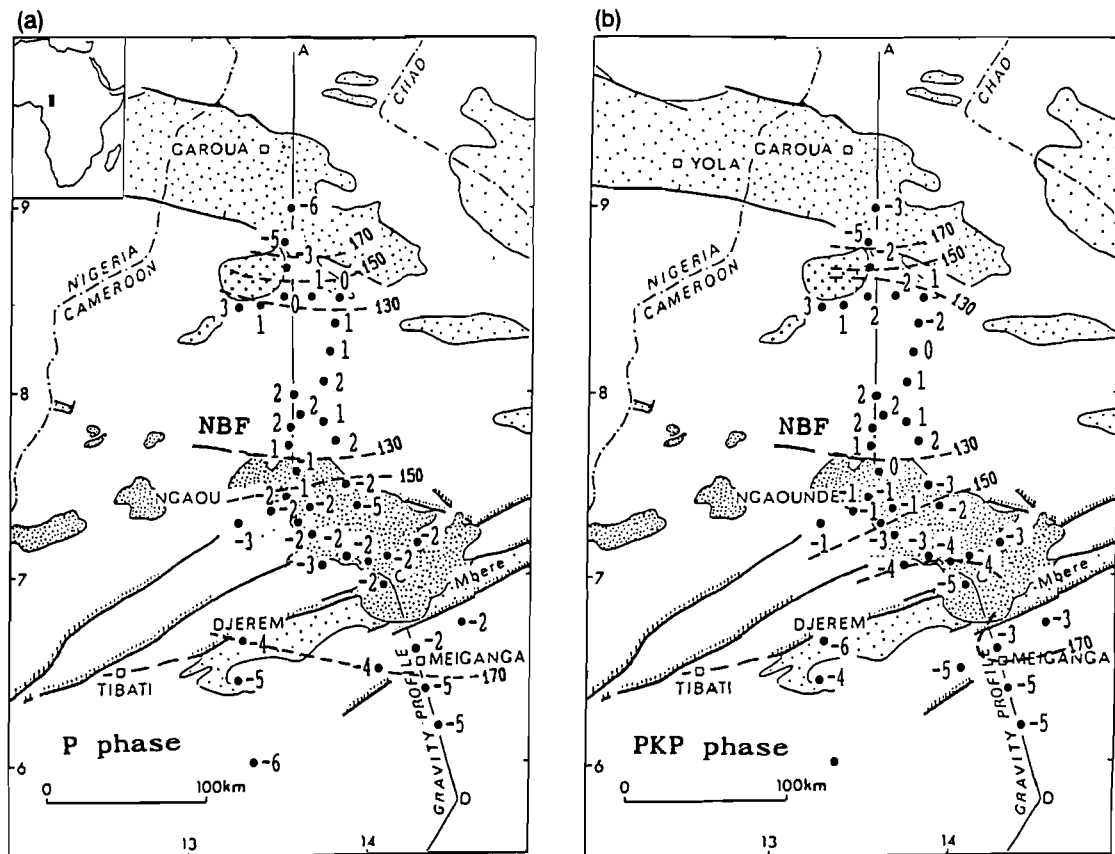


**Figure 2.** Representative average *P* (a) and *PKP* (b) residuals ( $\bar{R}_i$ ), in tenths of a second, and a corresponding model of the lithospheric thickness (isothickness contours, dashed curves), in kilometres. The residuals are corrected for crustal effects (Model B) and the averages  $\bar{R}_i$  are computed from steeply incident teleseismic waves homogeneously distributed with respect to their azimuths.

**Table 1.** Representative residuals and lithospheric thickness estimates.

S T A	Relative P residuals						Relative PKP residuals											
	model A			model B			model A' (DIST<180°)				model B' (DIST<180°)				model B' (DIST<140°)			
	$\bar{R}_i$ (s)	error	N l(km)	$\bar{R}_i$ (s)	error	N l(km)	$\bar{R}_i$ (s)	error	N l(km)	$\bar{R}_i$ (s)	error	N l(km)	$\bar{R}_i$ (s)	error	N l(km)	$\bar{R}_i$ (s)	error	N l(km)
1	0.06	±.03	16 123	-0.14	±.03	16 148	0.22	±.02	5 108	0.02	±.02	5 133	0.04	±.02	5 131			
2	0.02	.02	15 126	-0.14	.02	15 148	0.02	.01	4 127	-0.13	.01	4 147	-0.13	.01	4 146			
3	-0.01	.04	14 129	-0.21	.04	14 155	-0.08	.06	3 136	-0.28	.06	3 161	-0.26	.02	3 158			
4	-0.02	.02	16 130	-0.15	.02	16 149	0.02	.02	5 127	-0.12	.02	5 146	-0.09	.02	5 142			
5	-0.34	.04	16 160	-0.27	.04	16 160	-0.45	.03	5 171	-0.39	.03	5 171	-0.36	.03	5 168			
6	-0.18	.03	15 145	-0.21	.03	15 155	-0.23	.03	4 150	-0.26	.03	4 159	-0.24	.03	4 156			
7	-0.20	.10	16 147	-0.26	.10	16 159	-0.02	.09	3 130	-0.08	.09	3 142	-0.13	.12	3 146			
8	-0.03	.05	15 131	-0.16	.05	15 150	-0.02	.03	3 130	-0.14	.04	3 148	-0.04	.01	3 138			
9	-0.09	.03	16 137	-0.15	.03	15 149	-0.01	.02	5 129	-0.08	.03	5 142	-0.04	.03	5 138			
10	-0.01	.04	15 129	0.07	.04	15 128	-0.06	.03	4 134	-0.00	.03	4 135	0.01	.02	4 133			
11	0.08	.04	15 121	0.15	.03	15 121	-0.01	.00	5 129	0.05	.01	5 130	0.06	.02	4 128			
12	0.11	.02	16 118	0.18	.02	16 118	0.10	.02	5 119	0.16	.02	5 120	0.18	.01	5 117			
13	0.05	.02	16 123	0.12	.02	16 123	0.01	.03	4 128	0.07	.03	4 128	0.08	.03	4 126			
14	0.05	.01	15 123	0.12	.01	15 123	0.07	.01	5 122	0.13	.01	5 123	0.14	.02	5 121			
15	0.10	.02	15 119	0.17	.02	15 119	0.10	.05	5 119	0.16	.05	5 120	0.13	.03	5 122			
16	0.08	.03	16 121	0.15	.03	16 121	0.08	.01	5 121	0.15	.01	5 121	0.14	.01	5 121			
17	0.08	.03	15 115	0.21	.02	15 115	0.11	.02	5 118	0.17	.02	5 119	0.17	.02	5 118			
18	-0.64	.09	12 188	-0.56	.09	12 187	-0.33	.06	2 160	-0.27	.07	2 160	-0.19	-	1 152			
19	-0.55	.06	14 180	-0.48	.06	14 180	-0.56	.05	3 181	-0.48	.04	3 180	-0.52	.01	3 183			
20	-0.35	.09	12 161	-0.28	.09	12 161	-0.26	.05	2 153	-0.20	.05	2 153	-0.23	-	1 155			
21	-0.08	.05	14 136	-0.01	.05	14 136	-0.02	.03	3 130	0.06	.04	3 129	0.11	.01	3 123			
22	-0.03	.08	14 131	0.05	.08	14 130	0.16	.06	2 113	0.23	.06	2 113	0.25	.06	2 110			
23	0.02	.06	8 126	0.10	.06	8 125	-0.22	-	1 149	-0.15	-	1 149	-0.14	-	1 147			
24	0.18	.11	10 111	0.26	.11	10 110	0.19	.12	2 111	0.27	.09	2 109	0.19	.01	2 116			
25	0.00	.11	11 128	0.08	.11	11 127	0.04	-	1 125	0.10	-	1 125	0.12	-	1 123			
26	-0.10	.12	14 138	-0.03	.12	14 138	0.16	.06	3 113	0.24	.04	3 112	0.17	.07	3 118			
27	-0.27	.03	8 154	-0.24	.04	8 157	-0.29	.14	4 156	-0.26	.14	4 159	-0.26	.14	4 158			
28	-0.30	.08	8 156	-0.24	.08	8 157	-0.43	.06	4 169	-0.37	.06	4 170	-0.46	.05	4 177			
29	-0.23	.13	7 150	-0.20	.13	7 154	-0.29	.05	4 156	-0.27	.06	4 160	-0.24	.03	4 156			
30	-0.17	.07	8 144	-0.18	.07	8 152	-0.35	.07	3 161	-0.35	.07	3 168	-0.32	.04	3 164			
31	-0.28	.09	8 155	-0.22	.09	8 155	-0.56	.03	2 181	-0.50	.02	2 182	-0.57	.08	3 187			
32	-0.37	.24	6 163	-0.52	.25	6 184	-0.10	.02	4 138	-0.24	.03	4 157	-0.23	.01	4 155			
33	-0.27	.23	2 154	-0.20	.23	2 154	-0.35	-	1 161	-0.29	-	1 162	-0.70	.06	2 200			
34	-0.27	.11	6 154	-0.20	.11	6 154	-0.38	.03	3 164	-0.32	.03	3 165	-0.39	.04	3 171			
35	-0.53	.11	6 178	-0.46	.12	6 178	-0.58	.03	4 183	-0.52	.03	4 184	-0.54	.04	4 185			
36	-0.46	.09	6 171	-0.39	.09	6 171	-0.53	.02	3 178	-0.47	.02	3 179	-0.48	.04	3 179			
37	-0.60	.08	6 185	-0.54	.08	6 186	-0.55	-	1 180	-0.48	-	1 180	-0.54	.12	2 185			
38	-0.46	.07	7 171	-0.39	.07	7 171	-0.61	-	1 186	-0.55	-	1 186	-	-	-			
39	-0.61	.11	9 185	-0.53	.11	9 185	-0.47	.07	2 173	-0.40	.07	2 172	-0.42	-	1 173			
40	-0.65	.11	4 189	-0.57	.11	4 188	-	-	-	-	-	-	-	-	-			
BNG	-1.03	.14	15 225	-0.96	.14	15 225	-	-	-	-	-	-	-	-	-			
BCAO	-1.13	.25	13 234	-1.06	.25	13 234	-	-	-	-	-	-	-	-	-			

whose deep-mantle paths and focal regions differ substantially. For example, the *P* and *PKP* waves with the closest ray paths at the surface, i.e. those arriving in the same azimuth with incidence angles of 20° and 5°, respectively, are at depths of approximately 300 km that are 120 km apart in horizontal direction. The high degree of conformity of the *P* and *PKP* residuals (Table 1 and Fig. 2) strongly supports the idea that the source of the lateral variations on the representative average residuals is a consequence of velocity variations in the upper mantle, not very deep beneath the array.

Fairhead & Reeves (1977) assumed that one-third of the delay time variation arose from a 5 per cent negative velocity contrast between the lithosphere and asthenosphere. Similar to Poupinet (1979) and according to a seismological definition of the lithosphere (Sacks & Snoke 1984) we converted lateral variations of the directionally independent representative averages  $\bar{R}_i$  into a model with variable lithospheric thickness. We applied here a gradient of 9.4 km/0.1s for a residual–lithospheric-thickness relation, derived originally for Europe (e.g. Babuška *et al.* 1987a, 1988). This relation assumes that effects of lateral variations of the average velocity in the entire subcrustal lithosphere are much smaller than the effects arising from variations in lithospheric thickness, i.e. that they occur

mainly as a consequence of a negative velocity contrast between the lithosphere and asthenosphere. No assumptions on the velocity–depth distribution or on the lithosphere–asthenosphere velocity contrast were made.

A lithospheric thickness of 225 km beneath the BNG station (Fairhead & Reeves 1977) was taken as a reference depth for a model of the lithosphere–asthenosphere transition in the Adamawa region derived from the *P* residuals (Table 1 and Fig. 2). A mean error in the residuals of ±0.1 s corresponds approximately to a 10 km error in the inferred lithospheric thickness. Although the mean errors in residuals can be several hundredths (Table 1) of a second only, the real error in estimates of the lithospheric thickness is surely greater than the corresponding statistical error. In computing the relief on the bottom of the lithosphere from *PKP* waves we were not able to use the BNG station as a reference station owing to the lack of *PKP* arrivals reported to the ISC. Therefore, we fixed our relative scales for *PKP* and *P* waves at station 16, which is located in the central part of the array, with a flat lithospheric base (see the residuals in Fig. 2), and has a full azimuthal coverage of events and a small mean error for  $\bar{R}_i$  (see Table 1). To assure that the results are not influenced by a possible misidentification among the core phases, we repeated the calculations with a limit on epicentral distance (DIST <

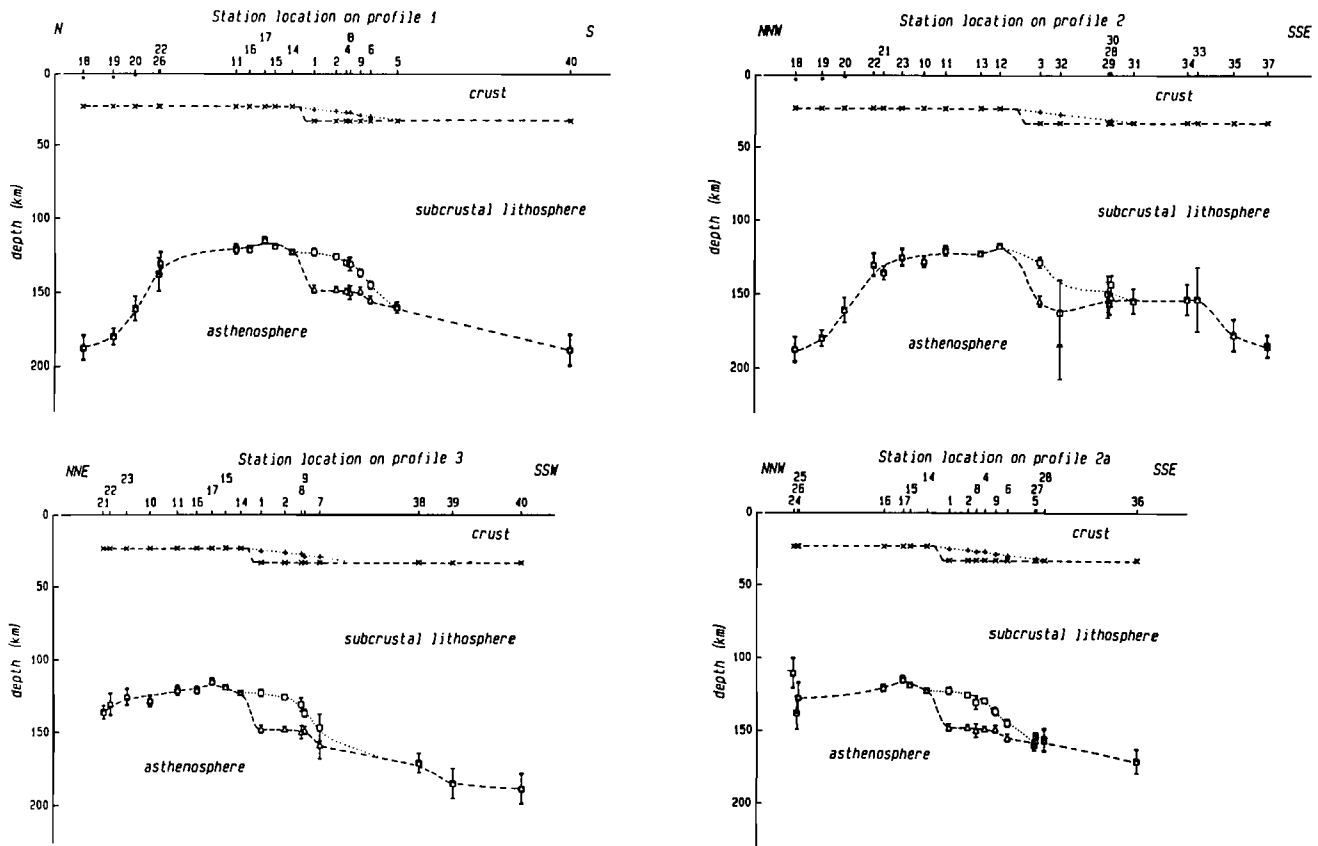


**Figure 3.** Cross-sections through the lithospheric models A and B derived from  $P$  residuals (Fig. 2a). Dashed lines and curves correspond to Model B, i.e. to the model with an abrupt change in M-discontinuity depth (crosses). Dotted lines and curves mark Model A, i.e. the model with a smooth change in M-discontinuity depth (pluses) to the south of the NBF (see text). Bars denote mean errors in lithospheric thickness estimates beneath the stations close the profiles. Small dots in the crust mark thicknesses of sediments for which the residuals were corrected. For more details see Table 1.

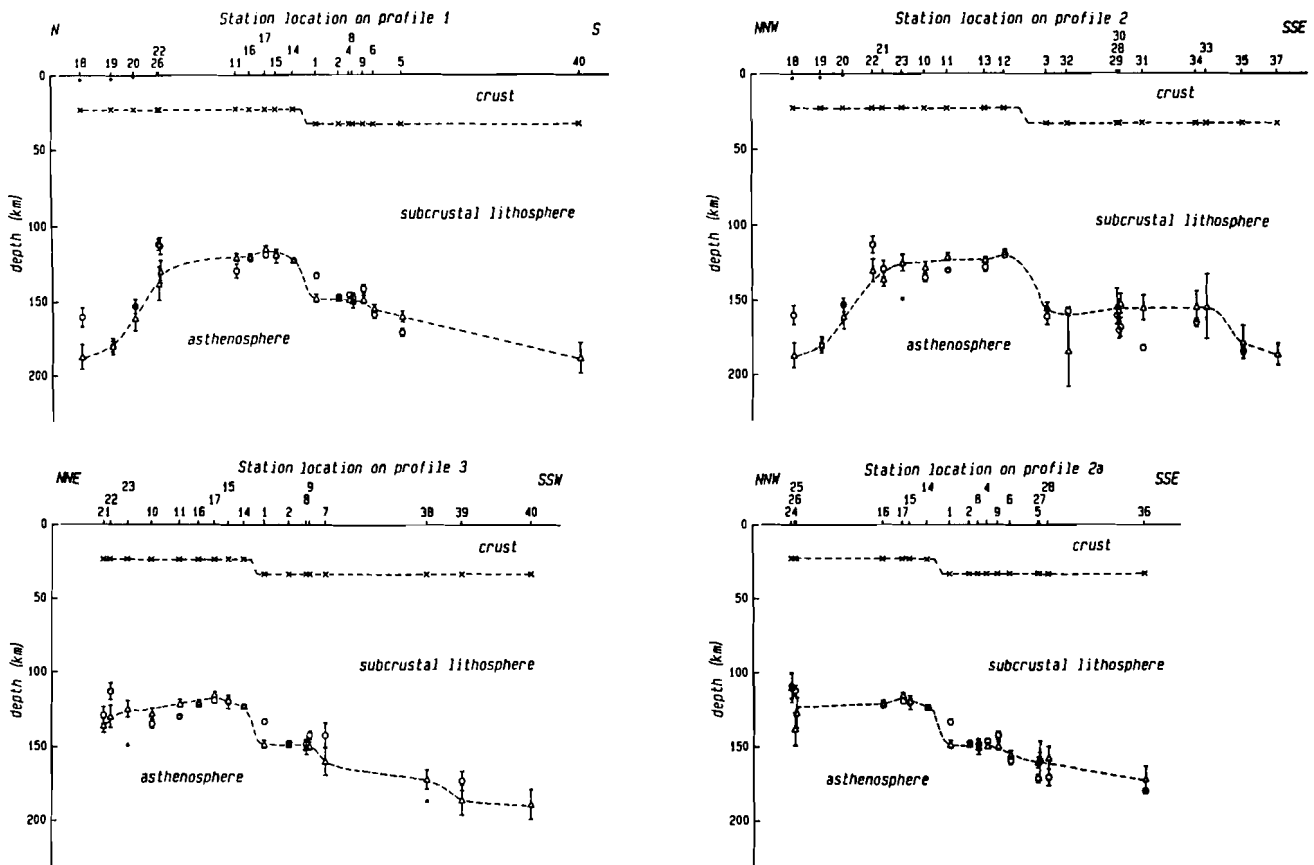
140°) and changed the grouping of events. No substantial effects on the residuals, and consequentially on lithospheric thickness, were found (see Table 1).

Figure 2 shows that the relief of the lithosphere–asthenosphere transition is shallower and flatter north of the Northern Boundary Fault (NBF) than in the northernmost part of the array. South of the NBF, the lithosphere is again substantially thicker. It is impossible to draw the contours for lithospheric thickness in the region reliably owing to the narrow, elongated shape of the array. Therefore, we demonstrate the undulation of the lithosphere–asthenosphere transition on several profiles (see Fig. 1) cutting the region in different directions. All five profiles (Figs 3–5) map a narrow shallowing of the lithosphere–asthenosphere transition in the central part of the array, north of the NBF. Whereas profiles 1, 2 and A'D' (Figs 3–5) indicate a thickening of the lithosphere both farther north and south of the NBF, profiles 2a and 3 demonstrate variations in lithospheric thickness mainly in the central and southern part of the array. Profiles 2 and 2a are parallel, whereas profile 3 was chosen perpendicular to the bipolar pattern of the spatial variations of the residuals (see Figs 7–9). The time delays interpreted here as the shallowing of the lithosphere–asthenosphere transition beneath the central part of the array were interpreted as a distinct low-velocity inhomogeneity in the 3-D velocity-perturbation

model computed down to a depth of 190 km (Dorbath *et al.* 1986).

The width of the asthenosphere upwelling depends strongly on the crustal model used (Fig. 3). Model A, which considers a smooth change of the crustal thickness across the NBF, broadens the upwelling to the south in comparison with Model B, where an abrupt change of crustal thickness is used. Taking into consideration the topography (Stuart *et al.* 1985) and the tectonic development of the region, as well as a pattern of the spatial variations of the residuals (see Section 5, Figs 7–9), Model B seems to be more probable than Model A. However, the gravity modelling in the following section offers another crustal model, referred to as a Model C, through which we achieve a closer fit of the computed and observed Bouguer anomalies (see Fig. 5).

Generally, there are only small deviations in the depths of the lithosphere–asthenosphere transition determined from the  $PKP$  residuals as compared with the model derived from the  $P$  residuals (Fig. 4). However, there is a remarkable misfit of the depths (about 17 km), which should not be ignored as it is observed for a pair of the most reliably determined values. This deviation between the models derived from  $P$  (models A and B) and  $PKP$  residuals (models A' and B') occurred for Station 1, situated very close to the south side of the NBF. The lithospheric models A' and B' use crustal models A and B, respectively. It



**Figure 4.** Cross-sections through lithospheric model B (dashed lines) derived from *P* residuals (dashed curves drawn through triangles) and the lithospheric depth estimates from the *PKP* residuals (Model B', circles). Half-size circles without the error bars (dots) correspond to the *PKP*-depth estimates based only on residuals of one source segment. For more details see Table 1 and Fig. 3 caption.

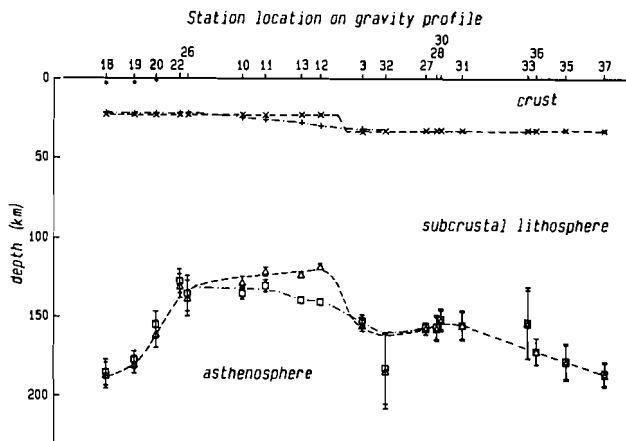


**Figure 5.** The input parameters of lithospheric model B for the gravity modelling (crosses and triangles interpolated by the dashed line and curve) along the gravity profile A'-D' (see Fig. 1). Model C, with a smooth change in the M discontinuity mainly to the north of the NBF and proposed during the gravity modelling, is marked by pulses and squares interpolated by the dot-dash line and curve (see text and captions to Figs 3 and 6b).

seems that the lithosphere beneath Station 1 derived from *PKP* residuals is too thin in comparison with other values. This is evident in models A and A', where there is broader

lithosphere shallowing beneath the central part of the array. For A' the value of  $108 \pm 2$  km beneath Station 1 is significantly above the level determined for surrounding stations, where the lithosphere-asthenosphere transition is at depths between 155 and 123 km beneath stations 14, 15, 16 and 17 to the north, and between 127 and 130 km beneath stations 2, 4 and 8 to the south (Table 1). We assume that the most probable cause of the discrepancy can be attributed to a non-vertical and complex continuation of the fault through the lithosphere, which thus affects very steep *PKP* differently from the less steep *P* waves that are incident from many azimuths.

#### 4 GRAVITY MODELLING

The input data for a starting model along a profile located as closely as possible to the gravity profile in order to compute the Bouguer gravity anomalies are the relief of the M discontinuity (Moho) from Stuart *et al.* (1985), and the depth of the lithosphere-asthenosphere transition from Fig. 5 (see also Fig. 9). Density contrasts of  $300 \text{ kg m}^{-3}$  between the crust and the subcrustal lithosphere, and  $-40 \text{ kg m}^{-3}$  between the lower lithosphere and asthenosphere were introduced into Model B (Fig. 6a). We need to explain by use of the model the approximately 100 mGal difference in the Bouguer anomaly observed north and south of the NBF. Fig. 6(a) demonstrates how the individual density zones of

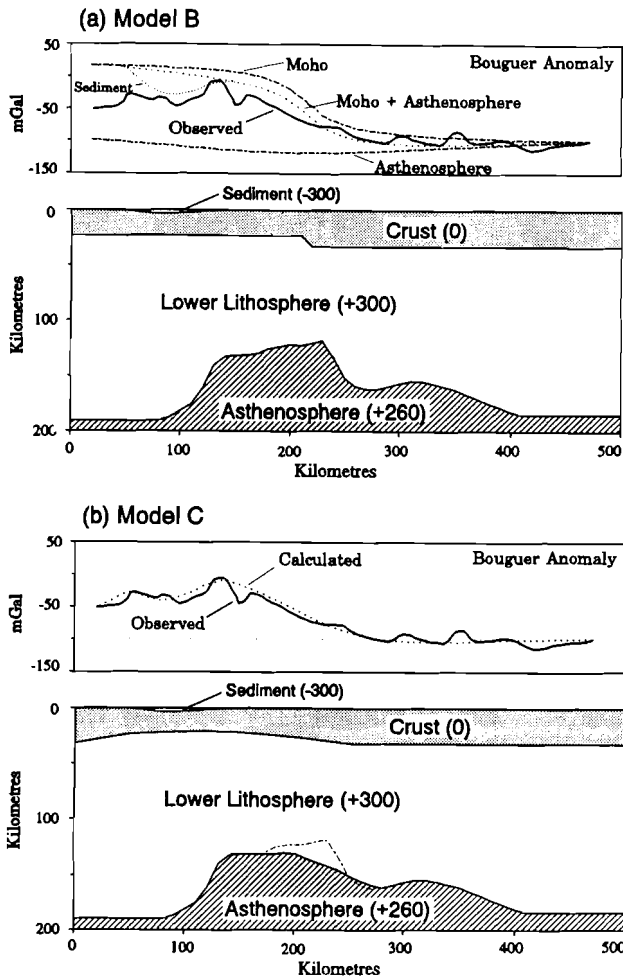


**Figure 6.** The observed Bouguer gravity anomalies (solid curves) and computed gravity anomaly curves for models B and C. Density contrasts are relative to normal crustal materials, in  $\text{kg m}^{-3}$ . The dashed and dotted curves (a) represent contributions to gravity due to the density contrasts assumed across individual boundaries according to Model B. (b) Lithospheric model in which relief of the M discontinuity (referred to as crustal model C in the text) is changed by trial and error method to achieve a closer fit of the calculated (total effect) and observed Bouguer anomalies. The dashed line on Model C represents the original configuration of the lithosphere–asthenosphere transition from Model B.

Model B contribute to the total gravity anomaly. Without taking into consideration effects of sediments beneath the northernmost part of the profile, the proposed crustal model B shows that the amplitude of the change of the observed Bouguer anomaly can be explained by the 10 km change in the M-discontinuity depth (e.g. Stuart *et al.* 1985). Although the shallowing of the lithosphere–asthenosphere transition is about 70 km, because it is narrow the resulting long-wavelength negative effect has very low amplitude ( $\approx 20$  mGal, Fig. 6a). Some of the short-wavelength misfit between the observed gravity anomaly and the computed anomaly (Moho + asthenosphere curve) can be improved by incorporating the rift sediments, with an average density of  $-300 \text{ kg m}^{-3}$  relative to the upper crust.

As the crustal effects are dominant in the gravity modelling due to a large density contrast, we proposed a

new crustal model (Fig. 6b) in which the configuration of the M discontinuity (Moho) is the only significant change from Model B. Instead of the abrupt change with depth, a smooth shallowing of the M discontinuity, slightly shifted to the north relative to the lithosphere–asthenosphere upwelling, was introduced. We refer to this model as crustal model C. The resulting computed gravity anomaly curve fits the observed Bouguer anomalies well (Fig. 6b).

As the crustal models A and B (see Section 3) used in residual computations affect the relief of the lithosphere–asthenosphere transition, namely the shape of its southern upwelling, we recomputed the residuals with the use of crustal corrections in Model C, which, contrary to Model A, smooths the abrupt change of the M discontinuity (Model B) to the north. As in the gravity modelling only the depths of the M discontinuity were changed (see Fig. 5); velocities and sediment thicknesses remained the same as in models A and B. The resulting model of the lithosphere–asthenosphere transition is smoother beneath the NBF than in the model that uses crustal model B, with an abrupt change of a depth of the M discontinuity beneath the NBF (Figs 5 and 6b).

An upwelling of the asthenosphere beneath rift regions is a typical phenomenon (e.g. the East African Rift, see Dahlheim, Davis & Achauer 1989). However, in the case of the Garoua Rift, the upwelling zone is very narrow. Whereas the crust–mantle boundary marks a compositional change, the lithosphere–asthenosphere transition is controlled by temperature and its effects on melting. Therefore, the age of the region can play an important role in the development of the lower boundary of the lithosphere. The Garoua Rift belongs to an old Cretaceous rift system running through South America, the Atlantic Ocean and Africa. As a result of cooling, the asthenosphere upwelling beneath old rifts would be attenuated. Therefore, the original upwelling was undoubtedly larger than that seen today through seismic delay-time methods.

## 5 SPATIAL VELOCITY VARIATIONS BENEATH THE ARRAY

Dorbath *et al.* (1986) found marked azimuthal variations of the relative residuals at both flanks of the array. The northern stations showed the most negative residuals between azimuths  $0^\circ$  and  $60^\circ$  and positive ones between  $60^\circ$  and  $110^\circ$ . Contrary to these observations, the southern stations showed the most negative residuals for southerly events. Twenty-one stations in the central part of the array had a much reduced or absent azimuthal variation.

Spatial variations of the residuals in dependence both on azimuths and epicentral distances, are depicted in Fig. 7, where the azimuth–incidence-angle dependent terms,  $\bar{R}_{i,k}$ , of the relative residuals are plotted in dependence on the azimuth and incidence angles at which P waves are assumed to arrive at the M discontinuity. Considering this map alongside selected examples of diagrams and in detail for all the diagrams of stations in the central part of the array (Fig. 8), we can see that the residual pattern changes relatively abruptly between stations 16 and 1. The change in orientation is limited to the close vicinity of the NBF, which separates the regions with opposite residual patterns.

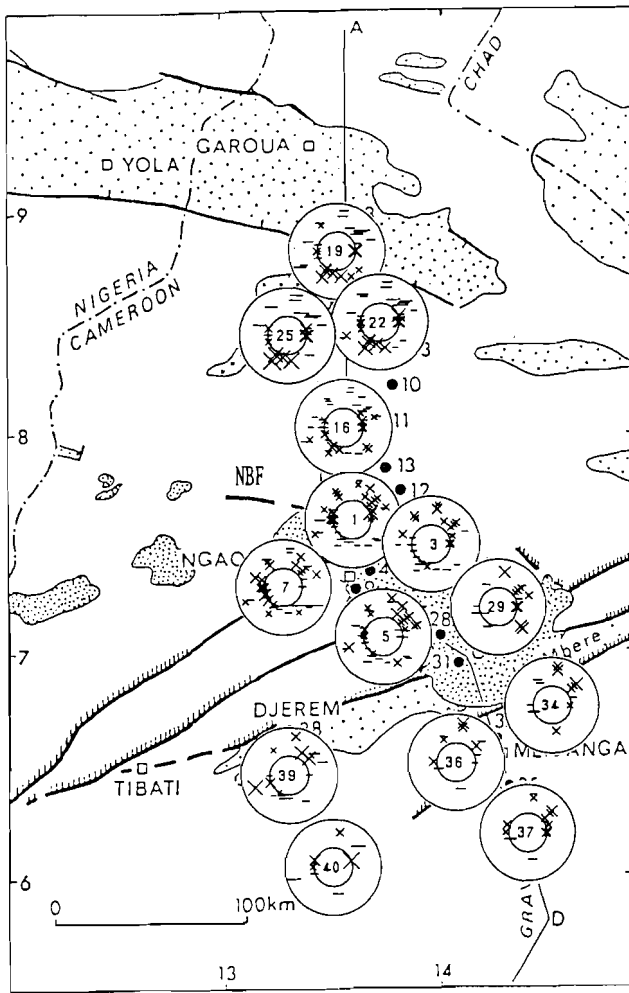


**Figure 7.** Sample diagrams of spatial variations of the azimuth-incidence-angle dependent terms  $\bar{R}_{i,k}$  of the  $P$  residuals plotted on a tectonic sketch map of the region around the array. Crosses denote positive values (i.e. late arrivals which indicate relatively low-velocity directions), and minuses denote negative values (i.e. early arrivals which indicate high-velocity directions). The size of the signs is proportional to the residual. The outer circle corresponds to an incidence angle of  $50^\circ$ , i.e. to epicentral distances of about  $20^\circ$ , the inner circle marks the  $20^\circ$  incidences at the  $M$  discontinuity at a reference depth of 33 km, with corresponding epicentral distances of  $100^\circ$ . A directional average  $\bar{R}_i$  represents a zero level at each diagram. The residual pattern changes close to the Northern Boundary Fault (NBF).

In Section 3 we showed (Fig. 3) how the crustal models used to correct the effects of the crustal part of the lithosphere affect the lithospheric thickness models of the region. Contrary to this, we found no dependence of the residual pattern on the crustal model used. The diagrams are identical, even for the stations in the close vicinity of the NBF. This means that the residual patterns (Figs 7–9) do express variations of the high  $P$ -velocity directions in the subcrustal lithosphere and that the effects of inhomogeneities either located in the crust or those that occur as a result of undulations of the lithosphere–asthenosphere transition are successfully minimized (Babuška et al. 1990).

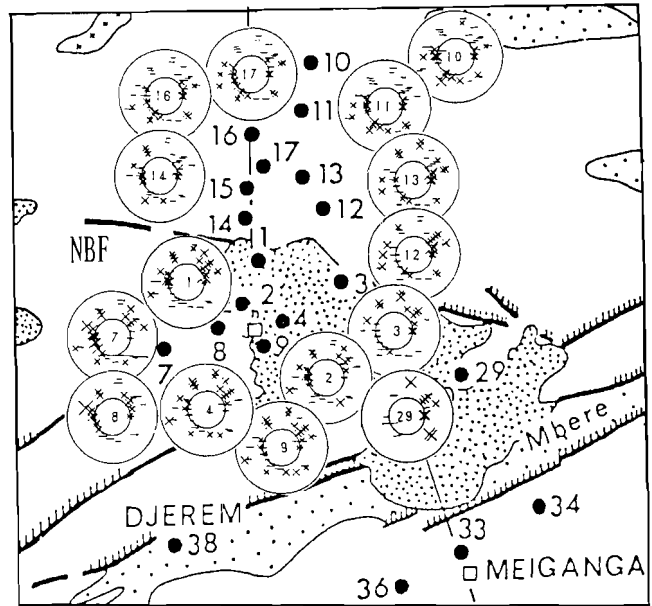


**Figure 8.** Spatial variations of the azimuth-incidence-angle dependent terms of the relative  $P$  residuals at stations close to the Northern Boundary Fault (NBF). For explanation of symbols see Fig. 7 caption.

## 6 DISCUSSION AND CONCLUSIONS

The tomographic study of the lithosphere beneath central Cameroon presented in Sections 3–5 showed that both the lithospheric thickness itself and the structure of its subcrustal part in relation to the orientation of the high- and low-velocity directions change in the close vicinity of the NBF. As the crustal thickness and the  $P$  velocities within the crust are relatively well determined for the investigated region (Stuart et al. 1985), we have used corrections to reduce the crustal effects. The observed variations of the  $P$  and  $PKP$  residuals are so large that only a small part can be explained by residuary (non-corrected) crustal effects, and their main source has to be sought in the mantle. As we observe the residual changes in the close vicinity of the Northern Boundary Fault, the effects cannot be situated too deep in the mantle. This is strongly supported by the fact that we observe approximately the same lateral variations of the static term (directionally independent averages  $\bar{R}_i$ ) for both  $P$  and  $PKP$  residuals, whose ray paths differ substantially in deeper parts of the mantle. Therefore, we assume most of the sources of the observed anomalies to be within the subcrustal lithosphere.

We emphasize that we use the same high-quality data as Dorbath et al. (1986), but we analyse them differently (see Section 2). The analysis of Dorbath et al. (1986) is based on azimuthal variations of the relative residuals and the traditional 3-D  $P$ -residual inversion. They divided the crust and uppermost mantle of the region into three blocks separated by subvertical boundaries striking ENE and reaching to depths greater than 190 km. The central block, which was over 100 km in width and had lower velocities by about 2 per cent compared with the adjacent blocks, roughly corresponds to the Central African Shear Zone.

In this paper we convert  $P$ -residual variations into lateral variations of the lithosphere–asthenosphere transition and

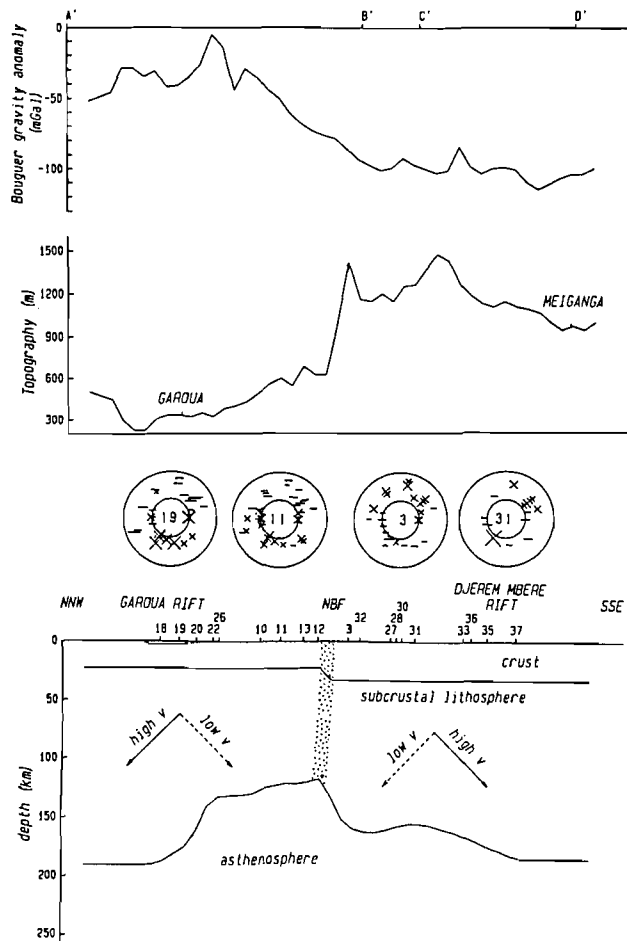


**Figure 9.** Cross-section through lithospheric model B, with Bouguer gravity profile (see Fig. 5), topography and the M discontinuity shown with a step of 10 km (from Stuart *et al.* 1985). The diagrams show examples of nearly opposite residual patterns (see Fig. 7 caption) for stations situated in blocks displaying different orientations of the inclined high- and low-velocity directions in the subcrustal lithosphere; marked schematically by long arrows with an angle of about  $45^\circ$ . Both blocks are separated by the Northern Boundary Fault (NBF); marked schematically by the steeply dipping stippled zone.

into inclined high- and low-velocity directions in the subcrustal lithosphere. Fig. 9 shows a cross-section through the model of the subcrustal lithosphere, in which the high- and low-velocity directions satisfying the observed spatial residual patterns are marked by arrows. Time delays, interpreted in the 3-D inversion of Dorbath *et al.* (1986) as the low-velocity central block, are interpreted here as a thinning of the lithosphere beneath the central part of the array (see also Figs 3 and 4). The northern end of the thinning agrees with a border between the northern high-velocity and the central low-velocity blocks, according to Dorbath *et al.* (1986). The width of the lithospheric thinning depends on the crustal model used (see Section 3). Model B, with an abrupt depth change in the M discontinuity close to the NBF, produces a more narrow asthenospheric upwelling, whereas the smooth crustal-thickness change (Model A) makes it slightly broader and shifts its southern boundary from the close vicinity of the

NBF about 50 km farther south, to a region of the proposed boundary between the central low-velocity and the southern high-velocity blocks (Dorbath *et al.* 1986). This means that the model of lithospheric thickness presented here, with the expressive narrow thinning beneath the central part of the array which coincides approximately with the Central African Shear Zone, refines the three-block lithospheric model of Dorbath *et al.* (1986).

On the other hand, spatial variations of the azimuth-incidence-angle dependent terms of the residuals (Figs 7–9) distinguished only two provinces with different—nearly opposite—orientations of high  $P$ -velocity directions. A boundary between these two regions coincides with the NBF, and its location is independent of the crustal model used. In the southern block the high  $P$  velocities dip to the south, in the northern block to the north. The blocks, which also differ in crustal and whole-lithospheric thicknesses, are separated by a relatively narrow zone that is shown to cut the entire lithosphere (Fig. 9). The findings point out the importance of the NBF and, together with the topographic relief, they indicate a preference for crustal model B (as opposed to Model A), with a more abrupt change of the M-discontinuity depth. A further modification based on gravity modelling (Model C) shows the crustal structure of the north side of the Garoua Rift to be more symmetrical with the south side (Fig. 6b). It seems that spatial variations of the azimuth-incidence-angle dependent terms of the residuals produce more detailed information on the inner structure of the subcrustal lithosphere than the azimuthal variations of the residuals, in which effects arising from inhomogeneities, such as the low-velocity central block, can suppress such information.

The most plausible explanation of the observed directional dependence of  $P$  velocities is a large-scale seismic anisotropy in the subcrustal lithosphere. An estimate of the anisotropy coefficient in the subcrustal lithosphere was based on rays that illuminate the lithosphere in opposite directions (e.g. see Babuška *et al.* 1984). We found only 2–5 per cent  $P$ -wave anisotropy, which explains the residual differences if we take into account the length of rays in the subcrustal lithosphere. The anisotropy has the inclined maximum  $P$ -velocity directions pointing to the south in provinces south of the NBF and to the north for northern provinces. An angle of  $45^\circ$  was taken to show schematically a dip angle for the maximum  $P$ -velocity direction (Fig. 9). The anisotropy coefficient found in the subcrustal lithosphere beneath central Cameroon is relatively low in comparison with values found in several regions in Europe (Babuška *et al.* 1984; Babuška, Plomerová & Spasov 1987b).

We have attempted to explain all the residual variations by the anisotropy only (P. Molnar, private communication, 1992). This consideration assumes no lateral variations of the lithospheric thickness, and the 0.7 s delay at the central part of the array relative to arrivals in its northern and southern flanks (Fig. 2) is explained only by reorientation of anisotropic structures in the 160 km thick subcrustal lithosphere. At least 6.3 per cent anisotropy is needed to fit the delays if the high-velocity directions are horizontal beneath the central part of the array, and inclined to the south in its southern part and to the north in its northern part (Fig. 9). This value, however, is higher than that

indicated from azimuth-incidence-angle dependent terms. Only subvertically oriented, high-velocity directions explain, in combination with subhorizontal ones, the delay for a weaker anisotropy of 3.7 per cent. Such orientations of anisotropic structures, however, do not fit the observed pattern (Figs 7–9) of the directional terms of the residuals (Babuška, Plomerová & Šílený 1993).

A preferred orientation of olivine grains, which originated in early stages of the creation of the oceanic lithosphere, is the most probable cause of the anisotropic structure of the subcrustal lithosphere. It is assumed that the original olivine orientation is preserved during the subduction of the oceanic lithosphere, from which an old continental nucleus grew in the past (Babuška & Plomerová 1989). The different orientations of *P* velocities in the subcrustal lithosphere beneath the southern and the northern part of the region thus indicate that both blocks probably originated in different tectonic settings and different regions, before coming together. The West African rift system may thus represent a reopening of the African Plate along an old accretionary suture zone (Fairhead & Binks 1991). The existence of such an old suture is supported by palaeomagnetic data for Pangea for Permian to Jurassic time (Smith & Livermore 1991). The data suggest that Africa must be broken into at least two fragments along the Benue Trough and its northern continuation.

#### ACKNOWLEDGMENTS

We are very grateful to Peter Molnar for his criticism and helpful discussions that improved the manuscript. Our thanks are also due to two anonymous reviewers for their comments and to P. Pajdušák who kindly cooperated during the *P* to *PKP* modification method.

#### REFERENCES

- Aki, K., Christofferson, A. & Husebye, E. S., 1977. Determination of the three dimensional seismic structure of the lithosphere, *J. geophys. Res.*, **82**, 277–296.
- Babuška, V. & Plomerová, J., 1989. Seismic anisotropy of the subcrustal lithosphere in Europe: another clue to recognition of accreted terranes?, in *Deep Structure and Past Kinematics of Accreted Terranes*, pp. 209–217, ed. Hillhouse, J. W., *Geophys. Monograph* 50, International Union of Geodesy and Geophysics, **5**.
- Babuška, V., Plomerová, J. & Šílený, J., 1984. Large-scale oriented structures in the subcrustal lithosphere of central Europe, *Ann. Geophys.*, **2**, 649–662.
- Babuška, V., Plomerová, J. & Šílený, J., 1987a. Structural model of the subcrustal lithosphere in central Europe, in *The Composition, Structure and Dynamics of the Lithosphere–asthenosphere system*, pp. 239–251, eds Froidevaux, C. & Fuchs, K., *Am. geophys. un. Geophys. Ser.* **16**.
- Babuška, V., Plomerová, J. & Spasov, E., 1987b. Deep structure of the lithosphere beneath the territory of Bulgaria, *Stud. Geophys. Geod.*, **31**, 266–283.
- Babuška, V., Plomerová, J. & Pajdušák, P., 1988. Lithosphere–asthenosphere in central Europe: models derived from *P* residuals, in *Proc. of the Fourth European Geotraverse (EGT) Project Workshop: The Upper Mantle*, pp. 37–48, eds Nolet, G. & Dost, B., European Science Foundation, Strasbourg.
- Babuška, V., Plomerová, J. & Granet, M., 1990. The deep lithosphere in the Alps: a model inferred from *P* residuals, *Tectonophysics*, **176**, 137–165.
- Babuška, V., Plomerová, J. & Šílený, J., 1993. Seismic anisotropy in deep continental lithosphere, *Phys. Earth planet. Inter.*, **78**, 167–191.
- Dahlheim, H. A., Davis, P. & Achauer, U., 1989. Teleseismic investigation of the East African Rift—Kenya. *J. Afr. Earth Sci.*, **8**, 461–470.
- De Almeida, F. F. & Black, R., 1967. Comparison structurale entre le nord-est du Bresil et l'Ouest africain, in *Symposium on Continental Drift*, Montivideo.
- Dorbath, L. & Montagner, J. P., 1983. Upper mantle heterogeneities in Africa deduced from Rayleigh wave dispersion, *Phys. Earth planet. Inter.*, **32**, 218–225.
- Dorbath, C., Dorbath, L., Fairhead, J. D. & Stuart, G. W., 1986. A teleseismic delay time study across the Central African Shear Zone in the Adamawa region of Cameroon, West Africa, *Geophys. J. R. astr. Soc.*, **86**, 751–766.
- Fairhead, J. D. & Binks, R. M., 1991. Different opening of the Central and South Atlantic Oceans and the opening of the West African rift system, *Tectonophysics*, **187**, 191–203.
- Fairhead, J. D. & Reeves, C. V., 1977. Teleseismic delay times, Bouguer anomalies and inferred thickness of the African lithosphere, *Earth planet. Sci. Lett.*, **36**, 63–76.
- Fitton, J. G., 1983. Active versus passive continental rifting: evidence from the West African rift system, *Tectonophysics*, **94**, 473–481.
- Knopoff, L. & Schlue, J. W., 1972. Raleigh wave phase velocities for path Addis Ababa–Nairobi, *Tectonophysics*, **15**, 157–163.
- Long, R. E., Backhouse, R. W., Maguire, P. K. H. & Sundar Lingham, K., 1972. The structure of East Africa using surface wave dispersion and Durham seismic array data, *Tectonophysics*, **15**, 165–178.
- Louis, P., 1970. *Contribution géophysique a la connaissance géologique du bassin du Lac Tchad*, Memoir 42, ORSTIM, Paris.
- Poupinet, G., 1979. On the relation between *P*-wave travel-time residuals and the age of continental plates, *Earth planet. Sci. Lett.*, **43**, 149–161.
- Sacks, I. S. & Snoke, J. A., 1984. Seismological determinations of the subcrustal continental lithosphere, in *Structure and Evolution of Continental Lithosphere*, pp. 3–39, eds Pollack, H. N. & Rama Murthy, V., Pergamon, Oxford.
- Smith, A. G. & Livermore, R. A., 1991. Pangea in Permian to Jurassic time, *Tectonophysics*, **187**, 135–179.
- Stuart, G. W., Fairhead, J. D., Dorbath, L. & Dorbath, C., 1985. A seismic refraction study of the crustal structure associated with the Adamawa Plateau and Garoua Rift, Cameroon, West Africa, *Geophys. J. R. astr. Soc.*, **81**, 1–12.
- Talwani, M., Worzel, J. L. & Landisman, M., 1959. Rapid gravity computations for two-dimensional bodies with application to the Mendocino submarine fracture zone. *J. Geophys. Res.*, **64**, 49–59.